Mineralogical Magazine (2020), **84**, 869–880
doi:10.1180/mgm.2020.75

CAMBRIDGE UNIVERSITY PRESS

Article

Vittinkiite, $MnMn_4[Si_5O_{15}]$, a member of the rhodonite group with a long history: definition as a mineral species

Nadezhda V. Shchipalkina[1]*, Igor V. Pekov[1], Nikita V. Chukanov[2], Natalia V. Zubkova[1], Dmitry I. Belakovskiy[3], Sergey N. Britvin[4] and Natalia N. Koshlyakova[1]

[1]Faculty of Geology, Moscow State University, Vorobievy Gory, Moscow, 119991 Russia; [2]Institute of Problems of Chemical Physics, Russian Academy of Sciences, Chernogolovka, Moscow region, 142432 Russia; [3]Fersman Mineralogical Museum of the Russian Academy of Sciences, Leninsky Prospekt 18-2, Moscow, 119071 Russia; and [4]Department of Crystallography, St Petersburg State University, University Embankment 7/9, 199034 St Petersburg, Russia

Abstract

The rhodonite-group mineral with the idealised, end-member formula $MnMn_4[Si_5O_{15}]$ and the crystal chemical formula $^{VII}M(5)Mn\ ^{VI}M(1–3)Mn_3\ ^{VII}M(4)Mn[Si_5O_{15}]$ (Roman numerals indicate coordination numbers) is defined as a valid mineral species named vittinkiite after the type locality Vittinki (Vittinge) mines, Isokyrö, Western and Inner Finland Region, Finland. Vittinkiite is an isostructural analogue of rhodonite, ideally $CaMn_4[Si_5O_{15}]$, with Mn^{2+} > Ca at the *M*(5) site. Besides Vittinki, vitiinkiite was found in more than a dozen rhodonite deposits worldwide, however, it is significantly less common in comparison with rhodonite. The mineral typically forms pink to light pink massive, granular aggregates and is associated with quartz, rhodonite, tephroite, pyroxmangite and Mn oxides. Vittinkiite is optically biaxial (+), with $\alpha = 1.725(4)$, $\beta = 1.733(4)$, $\gamma = 1.745(5)$ and $2V_{meas} = 75(10)°$ (589 nm). The chemical composition of the holotype (wt.%, electron microprobe) is: MgO 0.52, CaO, 0.93, MnO 51.82, FeO 1.26, ZnO 0.11, SiO_2 46.48, total 101.12. The empirical formula calculated based on 15 O apfu is $Mn_{4.71}Ca_{0.11}Fe_{0.11}Mg_{0.08}Zn_{0.01}Si_{4.99}O_{15}$. Vittinkiite is triclinic, space group $P\bar{1}$, with $a = 6.6980(3)$, $b = 7.6203(3)$, $c = 11.8473(5)$ Å, $\alpha = 105.663(3)$, $\beta = 92.400(3)$, $\gamma = 94.309(3)°$, $V = 579.38(7)$ Å^3 and $Z = 2$. The crystal structure is solved on a single crystal to $R_1 = 3.85\%$. Polymorphism of $MnSiO_3$ (rhodonite-, pyroxmangite-, garnet- and clinopyroxene-type manganese metasilicates) is discussed, as well as the relationship between vittinkiite and pyroxmangite, ideally $Mn_7[Si_7O_{21}]$, and the application of infrared spectroscopy for the identification of manganese pyroxenoids.

Keywords: vittinkiite, new mineral, rhodonite group, manganese silicate, inosilicate, pyroxenoid, $MnSiO_3$ polymorphism, crystal structure, Vittinge mines

(Received 12 August 2020; accepted 21 September 2020; Accepted Manuscript published online: 25 September 2020; Associate Editor: Oleg I Siidra)

Introduction

Rhodonite is a well-known pyroxenoid and typical rock-forming constituent of many manganese-rich rocks. The first mention of rhodonite appeared in the paper by Germar (1819), on the basis of data from Jasche who described it two years earlier (Jasche, 1817). This name was given initially to a rock formed by pinkish-red Mn-rich silicates (at present known as rhodonite and pyroxmangite), quartz, tephroite and Mn oxides. Somewhat later, the name rhodonite was transferred to the major manganese silicate of this rock which typically has a pink or red colour (ρόδον means rose in Greek). For a long time, several minerals with different chemical and crystal chemical features were all combined under the name rhodonite. A brief historical review is given by Shchipalkina *et al.* (2019b).

Some confusion with the term 'rhodonite' remained up to recent times, even after detailed elaboration of the crystal chemistry of manganese pyroxenoids. This is due to the absence of a clear definition of rhodonite as a mineral species with significant chemical variations, mainly in the Mn, Ca and Fe contents, in samples belonging to the rhodonite structure type; the situation was additionally complicated by the ordering of some cations in the rhodonite-type structure. In accordance with modern criteria in mineral nomenclature, such a situation cannot be described in the framework of a single mineral species, thus a mineral group needed to be established and defined. In 2019, we proposed a nomenclature for the rhodonite group and this proposal was accepted by the Commission on New Minerals, Nomenclature and Classification of the International Mineralogical Association (IMA–CNMNC) as Proposal 18-I (Miyawaki *et al.*, 2019).

According to the IMA-accepted nomenclature, the rhodonite group includes isostructural pyroxenoids with the general crystal chemical formula $^{M(5)}A^{M(1–3)}B_3\ ^{M(4)}C[Si_5O_{15}]$ in which the species-defining components are: *A* = Ca or Mn^{2+}, *B* = Mn^{2+} and *C* = Mn^{2+} or Fe^{2+} (Shchipalkina *et al.*, 2019b). The structural formula of rhodonite-group minerals can be written as $^{VI}M(1)\ ^{VI}M(2)\ ^{VI}M(3)\ ^{VI}M(4)\ ^{VII}M(5)[Si_5O_{15}]$ (Roman numerals mean coordination numbers of metal cations *M*) and simplified to $^{VII}M(5)\ ^{VI}M(1–4)[Si_5O_{15}]$. In the simplified formula, two types of *M* cations with different coordination numbers are distinguished. At present, three valid mineral species belonging to this group are known, namely

*Author for correspondence: Nadezhda V. Shchipalkina, Email: estel58@yandex.ru
Cite this article: Shchipalkina N.V., Pekov I.V., Chukanov N.V., Zubkova N.V., Belakovskiy D.I., Britvin S.N. and Koshlyakova N.N. (2020) Vittinkiite, $MnMn_4[Si_5O_{15}]$, a member of the rhodonite group with a long history: definition as a mineral species. *Mineralogical Magazine* **84**, 869–880. https://doi.org/10.1180/mgm.2020.75

rhodonite defined as $CaMn_4[Si_5O_{15}]$, ferrorhodonite with the idealised formula $CaMn_3Fe[Si_5O_{15}]$ (Shchipalkina *et al.*, 2017) and vittinkiite described in the present paper. A proposal on vittinkiite was submitted by us to the IMA–CNMNC in 2017, however, it could only be accepted as a mineral species after the approval of the nomenclature of the rhodonite group in August 2019. Vittinkiite (IMA 2017–082a, Shchipalkina *et al.*, 2019a) is defined as an analogue of rhodonite with the prevailing of Mn^{2+} over Ca at the *A* [= *M*(5)] site and, thus, with the idealised, end-member formula $MnMn_4[Si_5O_{15}]$. The minerals now known as rhodonite and vittinkiite were earlier joined under the general name 'rhodonite' and typically described with the simplified formula $MnSiO_3$, considering only the gross dominant metal cation Mn^{2+} and ignoring cation distribution between different *M* sites.

Vittinkiite can be named figuratively 'an old new mineral'. This rhodonite-type mineral with a low Ca content has been known for a long time, however, it is much rarer than rhodonite *sensu stricto*, the idealised end-member formula of which is $CaMn_4[Si_5O_{15}]$. Such a Ca-poor rhodonite-group mineral has been reported undeniably from two localities in Finland, namely Vittinge (Sundius, 1931) and Simsiö (Hietanen, 1938), the Taguchi manganese deposit in Aichi Prefecture, Japan (Momoi, 1964), the Xanthi area in Greece (Sapountzis and Christofides, 1982), and the Malosedel'nikovskoe, Kurganovskoe, Kozhaevskoe and Faizulinskoe manganese and rhodonite deposits in the Urals, Russia (Brusnitsyn, 2013). It is noteworthy that, based on the chemical data on Uralian rhodonite, Brusnitsyn and Zaitsev (2000) suggested distinguishing two separate mineral species with the idealised formulae $CaMn_4[Si_5O_{15}]$ and $MnMn_4[Si_5O_{15}]$ under the conventional names 'rhodonite-I' and 'rhodonite-II', respectively.

Earlier published representative chemical analyses of 'rhodonite' corresponding to vittinkiite (i.e. with Ca < 0.5 atoms per formula unit = apfu) are given in Table 1. The data on crystal structures of several Ca-poor rhodonite-type minerals (now defined as vittinkiite) and synthetic $MnMn_4[Si_5O_{15}]$ (Ohashi and Finger, 1975; Peacor *et al.*, 1978; Pertlik and Zahiri, 1999; Narita *et al.*, 1977) are summarised and discussed by Shchipalkina *et al.* (2019b).

Vittinkiite was named by us after the Vittinki (an old Swedish name is Vittinge) iron mines, Isokyrö, Western and Inner Finland Region, Finland. The choice of this name has a double reason: (1) the first published analysis of 'rhodonite' with Ca < 0.5 apfu (#2 in Table 1: Sundius, 1931) was from Vittinki; and (2) the Fersman Museum specimen cat#15061 that became the holotype is from the same locality.

Rhodonite from Vittinki (Vittinge) was first described in 1863 by Adolf Erik Nordenskiöld (Nordenskiöld, 1863). The specimen studied by us, which became the holotype of vittinkiite, is deposited in the systematic collection of the Fersman Mineralogical Museum of the Russian Academy of Sciences, Moscow under the catalogue No. 15061. It was acquired before 1926 from the collection of Adolf Erik Nordenskiöld (1832–1901) and catalogued as rhodonite in 1926. We believe that it is identical or close to the material described in Nordenskiöld (1863).

Besides data on the holotype vittinkiite, this present work provides data on several vittinkiite specimens from other localities studied by us and discusses the history of identification of two natural $MnSiO_3$ polymorphs: pyroxmangite $Mn_7[Si_7O_{21}]$ and vittinkiite $MnMn_4[Si_5O_{15}]$.

Experimental

Samples

Rhodonite-group minerals from the collection of the Fersman Mineralogical Museum were studied by electron microprobe analysis and infrared (IR) spectroscopy and/or powder X-ray diffraction (PXRD) was used to confirm they belonged to the rhodonite structural type. Among 60 samples studied from 30 worldwide localities, we found vittinkiite in nine specimens from six localities. These are specimens from Vittinki iron mines, Isokyrö, Finland (No. 15061, now the holotype of vittinkiite); New England Range, New South Wales, Australia (No. 61533); Ridder Mine (now Leninogorskiy Mine), NW Altai, Kazakhstan (No. 80484); Sultanuizdag, Uzbekistan (Nos. 78835, 78836 and 77378); Nozhiy Lake, Aginsk district, Zabaikal'sky Krai, Russia (No. 25677); and Tsang-Ping, Hebei, China (No. 58691) All these specimens are visually similar to each other. They consist of massive aggregates of pinkish vittinkiite associated with quartz, tephroite, black unspecified Mn oxides and sometimes pyroxmangite.

The samples of rhodonite, pyroxmangite and pyroxferroite used to obtain reference IR spectra originate from the collection of one of the coauthors (N.V.C.). Rhodonite from Långban, Sweden forms pink fine-grained aggregate in a skarn. Pyroxmangite samples from the Southern Faizulinskoe Mn deposit, South Urals, Russia and from the Razoare Mn deposit, Maramures, Romania occur as crimson granular aggregates. Mn-rich pyroxferroite from a metamorphosed xenolith of gneiss hosted by alkaline basalt of the Bellerberg paleovolcano, Eifel, Germany forms imperfect brownish-red crystals.

In the holotype specimen, vittinkiite is light pink with a white streak. It forms massive aggregates composed by tabular single-crystal grains up to 2 mm across associated intimately with quartz and pyroxmangite (Fig. 1). The lustre is vitreous. The mineral is translucent in aggregates and transparent in thin fragments. Cleavage is perfect on {201} and good on {021} and {210}. The density measured by flotation in heavy liquids (Clerici solutions) is 3.68(2) g cm^{-3}. The density calculated using the empirical formula is 3.737 g cm^{-3}.

In plane polarised light vittinkiite is pale pink to colourless, depending on grain thickness, and non-pleochroic. Vittinkiite is optically biaxial (+), with $\alpha = 1.725(4)$, $\beta = 1.733(4)$ and $\gamma = 1.745(5)$ (589 nm). 2V estimated by the curvature of the interference isogyre in conoscopic mode on the sections perpendicular to the optical axes is 75(10)°; $2V_{calc} = 79°$. Orientation: $Y \wedge b = 22°$. The dispersion of optical axes is weak, $r < v$.

Composition

Chemical data for vittinkiite were obtained using a Jeol JSM-6480LV scanning electron microscope equipped with an INCA-Wave 500 wavelength-dispersive spectrometer (WDS mode). The acceleration voltage was 20 kV, the beam current was 10 nA and the electron beam was defocused to 4 μm × 4 μm. The contents of other elements with atomic numbers higher than that of carbon are below detection limits. The standards used for quantitative analysis were diopside for Mg, wollastonite for Ca, ferrosilite for Fe and Si, pure Zn for Zn, and pure Mn for Mn. Analytical data are given in Tables 1 and 2.

Single-crystal X-ray diffraction

Single-crystal X-ray diffraction was performed using an Xcalibur S CCD diffractometer with Mo*K*α radiation (λ = 0.71073 Å).

https://doi.org/10.1180/mgm.2020.75 Published online by Cambridge University Press

Table 1. Chemical composition of vittinkiite and representative earlier published analyses.

Constituent	Vittinki (Vittinge), Finland	Bald Knob, North Carolina, USA	Simsiö, Finland	Taguchi, Aichi Pref., Japan	Xanthi, Greece	Malosedel'nikovskoe, deposit, Middle Urals, Russia	Kurganovskoe deposit, Middle Urals, Russia	Kozhaevskoe deposit, South Urals, Russia	Faizulinskoe deposit, South Urals, Russia
Wt.%									
MgO	0.12	1.56	1.05	0.53	1.41	0.27	0.22	0.38	0.18
CaO	1.60	3.64	2.87	1.53	1.24	2.96	1.76	3.60	2.24
MnO	46.28	44.88	49.55	49.85	50.23	49.73	50.41	47.08	50.54
FeO	3.70	3.74	1.06	1.92	0.29	-	0.41	1.95	1.42
ZnO	-	-	-	-	-	-	-	-	-
Al_2O_3	0.73	0.78	-	0.82	-	-	-	-	-
SiO_2	46.57	45.49	46.82	44.42	46.91	46.49	46.76	46.82	45.62
Total	99.00	100.09	101.35	99.07	100.08	99.51	99.56	99.83	100.00
Formula calculated on the basis of 15 O atoms									
Mg	0.02	0.25	0.17	0.09	0.23	0.04	0.04	0.06	0.03
Ca	0.18	0.41	0.32	0.18	0.14	0.34	0.20	0.41	0.26
Mn	4.24	4.08	4.46	4.64	4.56	4.56	4.62	4.29	4.66
Fe	0.33	0.34	0.09	0.18	0.03	-	0.04	0.18	0.13
Zn	-	-	-	-	-	-	-	-	-
Al	0.09	0.10	-	0.11	-	-	-	-	-
Si	5.04	4.89	4.98	4.88	5.03	5.03	5.05	5.03	4.96
Reference	Sundius (1931)	Ross and Kerr (1932)	Hietanen (1938)	Momoi (1964)	Sapountzis and Christofides (1982)	Brusnitsyn (2000)	Brusnitsyn (2000)	Brusnitsyn (2000)	Brusnitsyn (2013)

"-" indicates the content is below the detection limit.

Fig. 1. Rock consisting of vittinkiite (Vit), quartz (Q) and pyroxmangite (Pxm) from Vittinki (Vittinge) iron mines, Isokyrö, Finland (the holotype vittinkiite).

Data reduction was performed using *CrysAlisPro* Version 1.171.37.35 (Agilent Technologies, 2014). A total of 15,014 reflections within the sphere limited by θ = 34.97° were obtained. The experimental details of data collection and refinement values are shown in Table 3. After averaging of equivalent reflections, the experimental set contained 4017 reflections with $I > 2\sigma(I)$. The data on rhodonite obtained by Peacor and Niizeki (1963) was used for the initial model for the structure refinement. The structure was refined using the *JANA2006* suite of programs (Petříček *et al.*, 2006). Atomic scattering factors for neutral atoms together with anomalous dispersion corrections were taken from *International Tables for X-ray Crystallography* (Ibers and Hamilton, 1974). The final refinement cycles finished with $R_1 = 3.85\%$, $wR_2 = 6.50\%$ and GooF = 1.00 for all data. Fractional atomic coordinates, refined site-scattering values, equivalent atomic displacement parameters (U_{eq}), and anisotropic atomic displacement parameters U^{ij} are given in Table 4. The selected interatomic distances are presented in Table 5. The crystallographic information file has been deposited with the Principal Editor of *Mineralogical Magazine* and is available as Supplementary material (see below).

Powder X-ray diffraction data

Powder X-ray diffraction data (PXRD) were collected using a Rigaku R-AXIS Rapid II diffractometer (image plate), Co*K*α (λ = 1.79021 Å), 40 kV and 15 mA, rotating anode with the microfocus optics, Debye-Scherrer geometry, $d = 127.4$ mm and exposure = 15 min. The data were integrated using the software package *Osc2Tab* (Britvin *et al.*, 2017). Calculated intensities were obtained by means of *STOE WinXPOW* v. 2.08 program suite based on the atomic coordinates and unit-cell parameters obtained from the single-crystal data. Data are listed in Table 6.

Infrared spectroscopy

Samples for infrared spectroscopy were powdered, mixed with anhydrous KBr and pelletised (the ratio sample:KBr was 1:150 in mass proportion). The infrared absorption spectra of a transparent, homogeneous crystal of vittinkiite and reference samples of rhodonite, pyroxmangite and pyroxferroite were obtained using an ALPHA FTIR spectrometer (Bruker Optics) at a resolution of 4 cm^{-1}. A total of 16 scans were collected for each spectrum. The IR spectrum of an analogous pellet of pure KBr was used as a reference.

https://doi.org/10.1180/mgm.2020.75 Published online by Cambridge University Press

Table 2. Chemical composition of vittinkiite from the collection of the Fersman Mineralogical Museum RAS, our data.

Catalogue No.	Holotype: Vittinki (Vittinge), Finland 15061		New England Range, New South Wales, Australia 61533	Ridder Mine, NW Altai, Kazakhstan 80484	Sultanuizdag, Uzbekistan 78835	Nozhiy Lake, Zabaikal'sky Krai, Russia 25677	Tsang–Ping, Hebei, China 58691
	Mean*	Range					
Wt. %							
MgO	0.52	0.50–0.54	0.07	0.13	0.88	0.09	1.33
CaO	0.93	0.93–0.94	1.65	2.72	1.98	1.33	1.84
MnO	51.82	50.80–52.84	52.84	51.57	50.36	52.45	49.20
FeO	1.26	1.21–1.32	0.72	0.37	1.41	0.43	1.61
ZnO	0.11	0.10–0.12	–	–	0.16	0.12	0.10
SiO_2	46.48	45.98–46.98	46.61	46.85	46.68	46.68	46.88
Total	101.12		101.89	101.64	101.47	101.10	100.96
Formula calculated on the basis of 15 O apfu							
Mg	0.08		0.01	0.02	0.14	0.01	0.21
Ca	0.11		0.19	0.31	0.22	0.15	0.21
Mn	4.71		4.78	4.66	4.55	4.77	4.44
Fe	0.11		0.06	0.03	0.13	0.04	0.14
Zn	0.01		–	–	0.01	0.01	0.01
Σ *M* cations	5.02		5.04	5.02	5.05	4.98	5.01
Si	4.99		4.98	4.99	4.98	5.01	4.99

"–" indicates the content is below the detection limit. *For four analyses.

Results and discussion

Infrared spectroscopy

Bands in the IR spectrum of vittinkiite (Fig. 2a) and their assignments are (cm^{-1}, s – strong band, sh – shoulder): 1112, 1053s and 1020s, (Si–O stretching vibrations of the Si–O–Si bridges), 950s, 930sh, 915sh, 891s and 874 (Si–O stretching vibrations of apical Si–O bonds), 718, 693, 664, 578 and 559 (O–Si–O bending vibrations), 515, 492, 458s and 391 (lattice modes involving Si–O–Si bending and *M*···O stretching vibrations where *M* = Mn, Fe and Ca). The IR spectrum of vittinkiite is close to that of rhodonite (Fig. 2; see also Chukanov, 2014). Note that the intensity of the band in the range from 390 to 395 cm^{-1} in IR spectra of rhodonite-type minerals increases with the lowering of Ca content at the *M*5 site. Based on this observation, we assign this band to ^{M5}Mn···O stretching vibrations.

The other distinctive features of vittinkiite that distinguish it from rhodonite are a high intensity of the band at 950 cm^{-1} and shifts of all strong bands of Si–O stretching vibrations towards lower wavenumbers as compared to analogous bands of rhodonite (cm^{-1}): 1060 → 1053, 1026 → 1020, 950 → 949 and 898 → 891. These features are characteristic of all vittinkiite samples independent of their origin.

Table 3. Crystal data and refinement details for vittinkiite.

Crystal data	
Formula	$Mn_5Si_5O_{15}$
Temperature (K)	293
Crystal size (mm)	0.26 × 0.23 × 0.14
Crystal system	Triclinic
Space group	$P\bar{1}$
a (Å)	6.6980(3)
b (Å)	7.6203(3)
c (Å)	11.8473(5)
α (°)	105.663(3)
β (°)	92.400(3)
γ (°)	94.309(3)
V (Å^3)	579.38(4)
Z	2
Density, D_x (g cm^{-3})	3.74
Absorption, μ (mm^{-1})	5.80
Data collection	
Radiation, wavelength (Å)	Mo*K*α, 0.7107
Data collection method	ω
F(000)	628
θ range for data (°)	2.79 to 34.97
Index ranges	$-10 \le h \le 10$, $-11 \le k \le 12$, $-18 \le l \le 18$
Reflections/unique	15,014/4783
Observed reflections	4017 with $I > 2\sigma(I)$
R_{int}	3.85
Refinement	
Refinement method	Full-matrix least-squares on *F*
Weighting scheme	$w = 1/(\sigma^2\|F\| + 0.0016\ F^2)$
Goodness-of-fit on *F*	1.00
Final *R* indices*	$R_1 = 0.0385$; $wR_2 = 0.0650$
$\Delta\rho_{min}$ / $\Delta\rho_{max}$ (e^-/Å^3)	−0.59/0.57

*$R_1 = \Sigma||F_{obs}|-|F_{calc}||/\Sigma|F_{obs}|$; $wR_2 = \{\Sigma[w(|F_{obs}|-|F_{calc}|^2]/\Sigma[w|F_{obs}|^2]\}^{1/2}$; GoF = $\{\Sigma w(|F_{obs}|-|F_{calc}|)^2/(n-p)\}^{1/2}$ where *n* is the number of reflections and *p* is the number of refined parameters.

Crystal structure of vittinkiite

The crystal structure of rhodonite was first solved by Liebau *et al.* (1959). The rhodonite structure contains the chains of tetrahedra with a repeat unit $[Si_5O_{15}]$ and ribbons formed by edge-sharing metal-centred polyhedra *M*1, *M*2, *M*3, *M*4 and *M*5 (Fig. 3). The polyhedra *M*1, *M*2 and *M*3 are slightly distorted octahedra with mean cation–oxygen distances 2.21–2.23 Å, occupied predominantly by Mn. The polyhedron *M*4 is a strongly distorted octahedron with the shortest and the longest cation–oxygen distances in the ranges 1.95 to 1.99 Å and 2.77 to 2.91 Å, respectively. This site concentrates Fe, Mg and Zn (Peacor and Niizeki, 1963; Ohashi and Finger, 1975; Peacor *et al.*, 1978; Nelson and Griffen, 2005; Leverett *et al.*, 2008; Shchipalkina *et al.*, 2017). The shortest *M*4–O distances are observed in samples with the highest contents of cations smaller than Mn^{2+}, namely Mg^{2+} and Fe^{2+}. The site *M*5 has seven-fold coordination and mean a cation–oxygen distance in the range 2.40–2.42 Å and in most cases is occupied predominantly by Ca (usually, together with subordinate Mn). Mutual alignment of the polyhedral ribbons and chains of tetrahedra is shown in Fig. 3.

https://doi.org/10.1180/mgm.2020.75 Published online by Cambridge University Press

Table 4. Atom coordinates, site multiplicities (Q) and Wyckoff letter, displacement parameters (U_{eq}/Å^2) and anisotropic displacement parameters (Å^2) for vittinkiite

Site	*x/a*	*y/b*	*z/c*	*Q*	U_{eq}*	U^{11}	U^{22}	U^{33}	U^{12}	U^{13}	U^{23}
*M*1	0.9712(2)	0.8799(1)	0.8520(1)	2*i*	0.0109(1)	0.0091(2)	0.0115(2)	0.0126(2)	0.0006(2)	0.0011(2)	0.0039(2)
*M*2	0.8718(2)	0.6838(2)	0.5543(1)	2*i*	0.0114(1)	0.0112(2)	0.0118(2)	0.0114(2)	0.0002(2)	0.0011(2)	0.0036(2)
*M*3	0.8130(1)	0.4894(1)	0.2693(1)	2*i*	0.0112(1)	0.0103(2)	0.0116(2)	0.0121(2)	0.0003(2)	0.0004(2)	0.0034(2)
*M*4	0.7930(2)	0.2963(2)	0.9726(1)	2*i*	0.0136(2)	0.0148(3)	0.0174(3)	0.0110(2)	0.0053(2)	0.0032(2)	0.0061(2)
*M*5	0.6508(1)	0.0383(1)	0.7024(1)	2*i*	0.0155(2)	0.0154(3)	0.0122(2)	0.0180(3)	−0.0006(2)	0.0007(2)	0.0030(2)
*T*1	0.4953(1)	0.2201(1)	0.1248(1)	2*i*	0.0091(2)	0.0075(3)	0.0108(4)	0.0097(3)	0.0003(3)	0.0011(3)	0.0037(3)
*T*2	0.6369(1)	0.2603(1)	0.4677(1)	2*i*	0.0093(2)	0.0082(3)	0.0104(4)	0.0095(3)	−0.0003(3)	0.0019(3)	0.0030(3)
*T*3	0.7036(1)	0.4535(1)	0.7351(1)	2*i*	0.0092(2)	0.0085(3)	0.0100(4)	0.0094(3)	0.0002(3)	0.0017(3)	0.0028(3)
*T*4	0.7550(1)	0.7435(1)	0.0887(1)	2*i*	0.0097(2)	0.0091(4)	0.0110(4)	0.0095(4)	−0.0002(3)	0.0008(3)	0.0039(3)
*T*5	0.8476(1)	0.9229(1)	0.3452(1)	2*i*	0.0091(2)	0.0091(3)	0.0089(4)	0.0099(3)	0.0002(3)	0.0018(3)	0.0035(3)
O1	0.9584(3)	0.9564(3)	0.6797(2)	2*i*	0.0110(6)	0.007(1)	0.011(1)	0.014(1)	−0.002(1)	0.001(1)	0.003(1)
O2	0.8926(3)	0.5965(3)	0.7314(2)	2*i*	0.0117(6)	0.008(1)	0.012(1)	0.015(1)	−0.000(1)	0.002(1)	0.004(2)
O3	0.8916(3)	0.7474(3)	0.3882(2)	2*i*	0.0124(6)	0.015(1)	0.010(1)	0.012(1)	0.000(1)	0.001(1)	0.005(1)
O4	0.8048(3)	0.3995(3)	0.4354(2)	2*i*	0.0121(6)	0.011(1)	0.012(1)	0.013(1)	−0.001(1)	0.002(1)	0.006(2)
O5	0.8088(4)	0.5467(3)	0.0950(2)	2*i*	0.0140(7)	0.016(1)	0.011(1)	0.014(1)	0.001(1)	0.001(1)	0.005(2)
O6	0.7330(3)	0.2002(3)	0.1319(2)	2*i*	0.0110(6)	0.006(1)	0.012(1)	0.015(1)	0.001(1)	0.002(1)	0.005(1)
O7	0.7412(4)	0.3096(3)	0.8084(2)	2*i*	0.0147(7)	0.016(1)	0.015(1)	0.015(1)	0.000(1)	0.001(1)	0.008(1)
O8	0.6617(3)	0.9348(3)	0.8544(2)	2*i*	0.0120(6)	0.009(1)	0.012(1)	0.014(1)	−0.001(1)	0.001(1)	0.005(1)
O9	0.4469(3)	0.2556(3)	0.9954(2)	2*i*	0.0126(6)	0.010(1)	0.018(2)	0.009(1)	0.001(1)	−0.001(1)	0.006(1)
O10	0.5818(3)	0.7654(4)	0.5972(2)	2*i*	0.0156(7)	0.009(1)	0.022(1)	0.014(1)	−0.001(1)	−0.002(1)	0.006(1)
O11	0.9429(3)	0.8427(3)	0.0395(2)	2*i*	0.0113(6)	0.009(1)	0.012(1)	0.013(1)	−0.000(1)	0.002(1)	0.006(1)
O12	0.5177(3)	0.5771(3)	0.7818(2)	2*i*	0.0119(6)	0.009(1)	0.009(1)	0.015(1)	0.000(1)	0.002(1)	0.001(1)
O13	0.6180(4)	0.3176(3)	0.6090(2)	2*i*	0.0156(7)	0.015(1)	0.017(1)	0.010(1)	−0.001(1)	0.002(1)	−0.001(1)
O14	0.7111(4)	0.0527(3)	0.4380(2)	2*i*	0.0158(7)	0.020(1)	0.010(1)	0.017(1)	0.002(1)	0.009(1)	0.005(1)
O15	0.7032(3)	0.8601(3)	0.2216(2)	2*i*	0.0122(6)	0.010(1)	0.015(1)	0.011(1)	−0.001(1)	0.001(1)	0.004(1)

*U_{eq} is defined as one third of the trace of the orthogonalised U^{ij} tensor.

Based on e_{ref} values, coordination numbers and interatomic distances, the occupancies of cationic sites in holotype vittinkiite are as follows (assumed cation assignment is given in square brackets taking into account the electron microprobe data): *M*1, *M*2, and *M*3–Mn^{2+}, *M*4–Mn^{2+} with minor Mg^{2+} [$Mn_{0.94}Mg_{0.06}$], and *M*5–Mn^{2+} with minor Ca^{2+} [$Mn_{0.92}Ca_{0.08}$].

The main, species-defining difference between vittinkiite $^{M(5)}Mn^{M(1-3)}Mn_3\ ^{M(4)}Mn[Si_5O_{15}]$ and rhodonite $^{M(5)}Ca^{M(1-3)}Mn_3\ ^{M(4)}Mn[Si_5O_{15}]$ is the predominant cation at the *M*5 site, i.e. Mn^{2+} or Ca, respectively.

Table 5. Selected interatomic distances for cation sites in the crystal structure of vittinkiite.

*M*1–O6	2.131(1)	*M*3–O3	2.100(1)	*M*5–O10	2.121(1)
*M*1–O8	2.145(1)	*M*3–O2	2.123(1)	*M*5–O7	2.135(1)
*M*1–O11	2.176(1)	*M*3–O5	2.223(1)	*M*5–O8	2.152(1)
*M*1–O2	2.254(1)	*M*3–O4	2.252(1)	*M*5–O1	2.203(1)
*M*1–O1	2.270(1)	*M*3–O12	2.255(1)	*M*5–O15	2.666(1)
*M*1–O11	2.326(1)	*M*3–O6	2.368(1)	*M*5–O13	2.669(1)
<*M*1–O>	2.217	<*M*3–O>	2.220	*M*5–O14	2.813(1)
				<*M*5–O>	2.393
*M*2–O10	2.124(1)	*M*4–O7	1.992(1)		
*M*2–O3	2.157(1)	*M*4–O5	2.053(1)		
*M*2–O1	2.221(1)	*M*4–O11	2.119(1)		
*M*2–O4	2.243(1)	*M*4–O6	2.241(1)		
*M*2–O4	2.309(1)	*M*4–O9	2.352(1)		
*M*2–O2	2.367(1)	*M*4–O8	2.788(1)		
<*M*2–O>	2.237	<*M*4–O>	2.258		
*T*1–O8	1.597(1)	*T*2–O10	1.599(1)	*T*3–O7	1.599(1)
*T*1–O6	1.611(1)	*T*2–O4	1.615(1)	*T*3–O2	1.616(1)
*T*1–O9	1.650(1)	*T*2–O13	1.625(1)	*T*3–O13	1.624(1)
*T*1–O12	1.651(1)	*T*2–O14	1.645(2)	*T*3–O12	1.642(1)
<*T*1–O>	1.627	<*M*1–O>	1.621	<*T*3–O>	1.620
*T*4–O5	1.589(1)	*T*5–O3	1.596(1)		
*T*4–O11	1.628(1)	*T*5–O1	1.618(1)		
*T*4–O9	1.647(1)	*T*5–O14	1.629(1)		
*T*4–O15	1.650(1)	*T*5–O15	1.656(1)		
<*T*4–O>	1.628	<*T*5–O>	1.625		

Polymorphism of $MnSiO_3$

Four polymorphs of a manganese metasilicate with the simplified end-member formula $MnSiO_3$ are known. They belong to the rhodonite, pyroxmangite (Narita *et al.*, 1977), garnet (Fujino *et al.*, 1986) and clinopyroxene (Tokohami *et al.*, 1979) structure types. These four compounds demonstrate the following polymorphic transformations accompanied by a regular increase in the density of crystal structures and change in coordination numbers (given in Roman numerals) of Mn and Si with expansion of SiO_4 tetrahedra and compression of Mn-centred octahedra (Fig. 4): rhodonite $^{VII(M5)}Mn^{VI(M1-4)}Mn_4[^{IV}Si_5O_{15}]$ (space group $P\bar{1}$) → pyroxmangite $^{VII(M1-2)}Mn^{VI(M3-7)}Mn_5[^{IV}Si_7O_{21}]$ ($P\bar{1}$) → synthetic clinopyroxene $^{VII(M2)}Mn^{VI(M1)}Mn[^{IV}Si_2O_6]$ ($P2_1/c$) → synthetic tetragonal garnet $^{VIII}Mn_3^{VI}Mn^{VI}Si[^{IV}SiO_4]_3$ ($I4_1/a$) (Akimoto and Syono, 1972; Momoi, 1974; Fujino *et al.*, 1986). The comparative data for these polymorphs are given in Table 7.

The repeat unit in pyroxenoids increases with the decrease in size of octahedrally coordinated cations, e.g. as a consequence of the main components Ca – Mn – Mg in the pyroxenoid series wollastonite – bustamite – rhodonite – pyroxmangite (Liebau, 1962; Takeuchi, 1977, and references therein). The composition of these $MnSiO_3$ polymorphs remains stable, but the transformation from the rhodonite-type to clinopyroxene-type crystal structure occurs through a compound with pyroxmangite structure type. This can be defined by the controlling factor of pressure that acts due to the effect of a smaller cation (for example, Mg in the $MnSiO_3$–$MgSiO_3$ system). The relationship between pyroxenoids (wollastonite, bustamite, rhodonite and pyroxmangite structural types) and pyroxenes has been the focus of many researchers (Burnham, 1971; Morimoto, 1966; Narita, 1973; Koto *et al.*, 1976; Pinckney and Burnham, 1988; Henry, 1998)

https://doi.org/10.1180/mgm.2020.75 Published online by Cambridge University Press

Table 6. Powder X-ray diffraction data (*d* in Å for Co*Kα* radiation) for vittinkiite*.

I_{meas}	I_{calc}	d_{meas}	d_{calc}	*h k l*	I_{meas}	I_{calc}	d_{meas}	d_{calc}	*h k l*	I_{meas}	I_{calc}	d_{meas}	d_{calc}	*h k l*
4	2	11.38	11.383	0 0 1	7	3	2.362	2.366	0 $\bar{3}$ 3	3	2	1.519	1.522	1 $\bar{3}$ 7
9	7	7.08	7.097	0 $\bar{1}$ 1		3		2.355	$\bar{2}$ 1 3		2		1.517	4 $\bar{1}$ 3
6	2	5.68	5.692	0 0 2	5	4	2.304	2.304	$\bar{1}$ $\bar{3}$ 1	4	4	1.513	1.512	1 $\bar{4}$ 6
26	19	4.739	4.749	$\bar{1}$ $\bar{1}$ 1		1		2.294	$\bar{1}$ $\bar{3}$ 2		4		1.505	$\bar{2}$ $\bar{2}$ 7
7	2	4.471	4.466	$\bar{1}$ 1 1		1		2.277	0 0 5	4	2	1.500	1.500	$\bar{2}$ 0 7
7	1	4.250	4.196	1 0 2		1		2.271	$\bar{1}$ 2 3	4	2	1.492	1.491	$\bar{1}$ 1 7
12	6	4.123	4.129	1 $\bar{1}$ 2		4		2.259	0 3 1		6		1.482	2 2 5
9	5	3.810	3.823	0 $\bar{1}$ 3		1		2.257	$\bar{1}$ $\bar{1}$ 5	23	15	1.478	1.478	3 $\bar{3}$ 5
3	3	3.651	3.654	0 2 0		1		2.240	$\bar{2}$ $\bar{2}$ 3	6	2	1.470	1.469	$\bar{1}$ 3 5
18	19	3.543	3.549	0 $\bar{2}$ 2	24	19	2.236	2.237	$\bar{2}$ 0 4	7	1	1.457	1.458	$\bar{1}$ $\bar{5}$ 2
6	4	3.399	3.404	1 $\bar{2}$ 1	**32**	**24**	**2.226**	**2.225**	**0 $\bar{2}$ 5**	7	3	1.454	1.452	$\bar{1}$ $\bar{5}$ 3
	6		3.343	$\bar{1}$ $\bar{1}$ 3	**40**	**34**	**2.180**	**2.181**	**$\bar{3}$ 1 0**					
42	**12**	**3.332**	**3.333**	**$\bar{1}$ 2 0**	7	5	2.153	2.154	3 0 1	9	9	1.432	1.434	$\bar{2}$ 2 6
14	10	3.251	3.256	$\bar{2}$ 0 1	15	14	2.116	2.116	$\bar{1}$ $\bar{2}$ 5		3		1.433	$\bar{3}$ 4 1
	5		3.231	0 2 1	20	23	2.078	2.079	1 3 1	21	18	1.424	1.425	4 2 1
9	6	3.206	3.209	1 0 3	8	6	2.064	2.065	2 $\bar{2}$ 4		13		1.423	$\bar{1}$ $\bar{5}$ 4
61	**37**	**3.138**	**3.141**	**$\bar{2}$ 1 0**	5	2	2.053	2.052	$\bar{2}$ 1 4	5	4	1.412	1.411	2 $\bar{5}$ 3
28	**17**	**3.077**	**3.073**	$\bar{1}$ $\bar{2}$ **2**	2	1	2.022	2.025	2 2 2	5	3	1.399	1.399	3 0 6
	2		3.044	0 1 3	3	2	2.001	2.004	$\bar{2}$ 2 3	7	9	1.388	1.387	$\bar{4}$ $\bar{1}$ 5
	1		3.026	$\bar{1}$ 2 1	3	4	1.980	1.980	3 $\bar{2}$ 1	5	3	1.374	1.374	1 0 8
29	**25**	**2.987**	**2.984**	**$\bar{2}$ 1 1**	4	3	1.941	1.939	$\bar{2}$ 0 5		4		1.349	$\bar{3}$ $\bar{2}$ 7
79	**54**	**2.958**	**2.964**	**$\bar{2}$ $\bar{1}$ 1**	11	4	1.890	1.895	2 $\bar{1}$ 5	4	1	1.341	1.341	$\bar{4}$ 1 5
95	**79**	**2.935**	**2.938**	**0 $\bar{1}$ 4**	11	4	1.862	1.868	3 1 2		2		1.339	$\bar{4}$ $\bar{2}$ 5
3	2	2.864	2.867	$\bar{1}$ 1 3	4	2	1.844	1.847	$\bar{1}$ $\bar{2}$ 6		3		1.333	$\bar{4}$ $\bar{3}$ 3
	2		2.818	2 $\bar{1}$ 2	14	4	1.826	1.826	$\bar{2}$ 3 2	5	2	1.331	1.331	2 1 7
9	7	2.804	2.806	$\bar{2}$ $\bar{1}$ 2	2	3	1.805	1.804	$\bar{1}$ 4 0		2		1.329	$\bar{1}$ 3 6
	1		2.798	2 0 2	3	5	1.791	1.791	$\bar{1}$ $\bar{4}$ 2	3	4	1.321	1.321	$\bar{2}$ $\bar{5}$ 4
	7		2.778	$\bar{1}$ $\bar{2}$ 3	1	2	1.777	1.762	$\bar{1}$ $\bar{4}$ 3	3	6	1.316	1.315	3 $\bar{1}$ 7
100	**100**	**2.749**	**2.751**	**0 2 2**	6	2	1.748	1.746	3 $\bar{1}$ 4		2		1.311	$\bar{3}$ 2 6
5	3	2.678	2.680	1 1 3	23	25	1.724	1.725	0 1 6		2		1.307	3 4 1
28	**27**	**2.655**	**2.659**	**1 $\bar{1}$ 4**	14	10	1.691	1.688	$\bar{1}$ $\bar{3}$ 6		2		1.303	$\bar{2}$ $\bar{4}$ 7
	1		2.637	$\bar{1}$ 2 2	8	10	1.680	1.678	$\bar{2}$ 3 3	4	1	1.302	1.302	2 3 5
	2		2.620	0 $\bar{2}$ 4	17	19	1.664	1.664	$\bar{4}$ 0 1		2		1.295	$\bar{2}$ 2 7
20	28	2.597	2.598	2 $\bar{2}$ 1	4	7	1.653	1.651	$\bar{3}$ $\bar{1}$ 5	7	7	1.291	1.290	3 $\bar{5}$ 3
	1		2.535	$\bar{2}$ $\bar{1}$ 3	7	9	1.639	1.638	1 1 6		2		1.278	4 $\bar{3}$ 5
	4		2.528	0 $\bar{3}$ 1	2	5	1.626	1.626	0 0 7		3		1.268	5 $\bar{2}$ 2
11	19	2.500	2.501	0 $\bar{3}$ 2	10	11	1.601	1.600	$\bar{2}$ 4 1		2		1.262	$\bar{4}$ 4 1
	3		2.459	1 2 2	9	9	1.585	1.585	$\bar{3}$ 3 2	7	4	1.245	1.244	1 $\bar{6}$ 4
14	13	2.444	2.447	2 1 2		5		1.583	$\bar{3}$ $\bar{3}$ 3	8	6	1.237	1.237	4 1 5
8	6	2.425	2.427	2 0 3	9	4	1.565	1.563	$\bar{4}$ 0 3	7	2	1.220	1.219	5 $\bar{3}$ 1
	2		2.419	$\bar{2}$ $\bar{2}$ 1	11	5	1.545	1.545	2 4 0					
	2		2.392	1 $\bar{3}$ 2		3		1.544	0 $\bar{4}$ 6					
	3		2.374	$\bar{2}$ $\bar{2}$ 2										

* For the calculated pattern, only reflections with intensities ≥1 are given.
The strongest lines are given in bold

who report several approaches to the interpretation of causes and triggers of their reversible transitions.

Only two of the above-discussed polymorphs of $MnSiO_3$ are found in nature, namely pyroxenoids with different periodicities of the silicate chain Si_nO_{3n}, vittinkiite, ideally $MnMn_4[Si_5O_{15}]$, and pyroxmangite, ideally $Mn_7[Si_7O_{21}]$. The rhodonite-type pyroxenoid, i.e. vittinkiite, is considered as a relatively low-pressure polymorph of $MnSiO_3$ whereas pyroxmangite is a high-pressure modification. For pure $MnSiO_3$, the transformation from the rhodonite-type form (vittinkiite) to the pyroxmangite-type form occurs at a pressure of 3 kbar and temperature ~350–400°C, though pyroxmangite can be metastable at low temperature and atmospheric pressures (Maresch and Mottana, 1976). This has been confirmed indirectly by pyroxmangite found originating from cavities in effusive rocks of the Eifel volcanic region, Germany (Shchipalkina *et al.*, 2016). The heating experiments undertaken by Aikawa (1979) show that $MnSiO_3$ with the pyroxmangite structure can exist metastably in the temperature range 400–1000°C, due to the high-activation energy of the pyroxmangite → 'rhodonite' (i.e. vittinkiite) transformation. According to high-pressure and high-temperature experiments by Akimoto and Syono (1972), the $MnSiO_3$ polymorphs with clinopyroxene ($P2_1/c$) and garnet structures ($I4_1/a$) appeared at pressures higher than 60 and 125 kbar, respectively. A complete phase diagram for the four $MnSiO_3$ polymorphs was reported by Akimoto and Syono (1972).

The effects of isomorphous substitutions on the stability of rhodonite- and pyroxmangite-type crystal structures and on *PT* conditions of the transformations rhodonite ↔ pyroxmangite were examined experimentally by Ito (1972) for the $MnSiO_3$–$MgSiO_3$ system. The influence of different impurities on the stability of these two structural types was also discussed by Pinckney and Burnham (1988), though that work concentrates mainly on the Mn–Mg substitutions. The general approximation of effects of substitutions of Mn for Ca, Mg and Fe in $MnSiO_3$ was reported by Maresch and Mottana (1976). According to their data, Fe^{2+} and Mg cations, smaller than Mn^{2+}, stabilise the pyroxmangite-type structure whereas Ca stabilises the rhodonite-type structure.

https://doi.org/10.1180/mgm.2020.75 Published online by Cambridge University Press

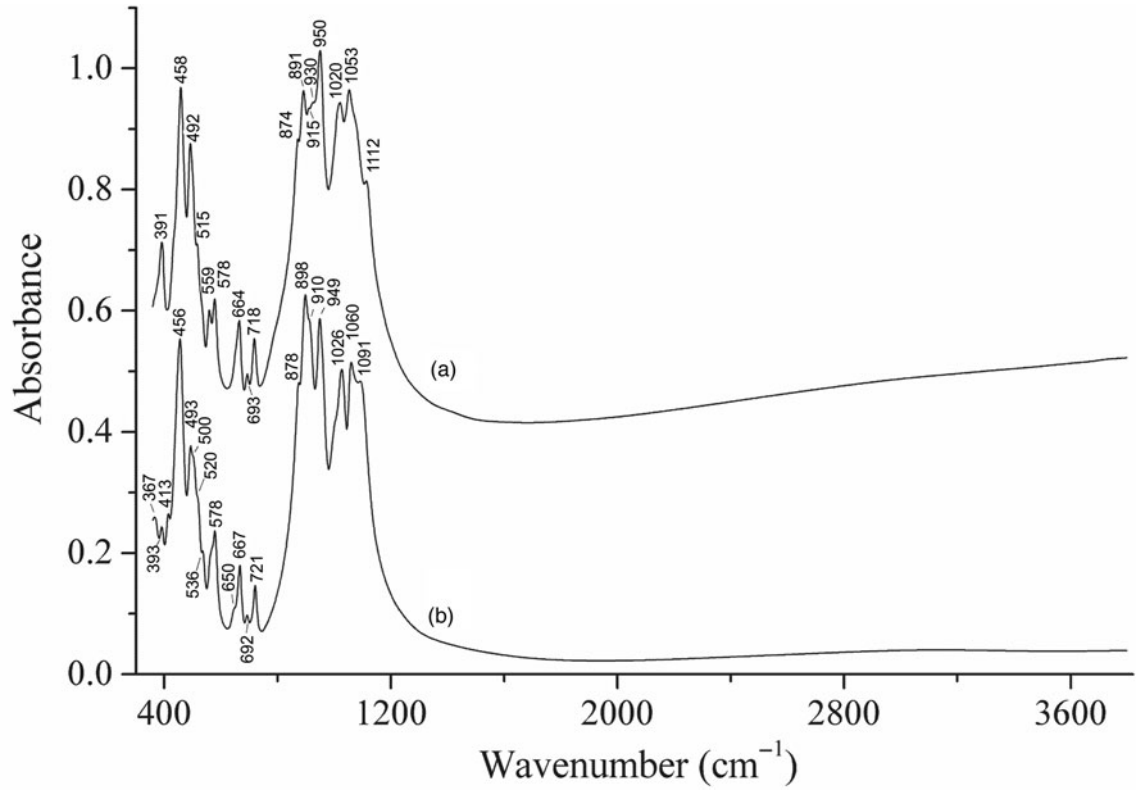

Fig. 2. Infrared absorption spectra of (*a*) the holotype vittinkiite and (*b*) rhodonite with the composition $Ca_{0.9}Mn_{3.7}Mg_{0.4}(Si_5O_{15})$ from Långban, Sweden.

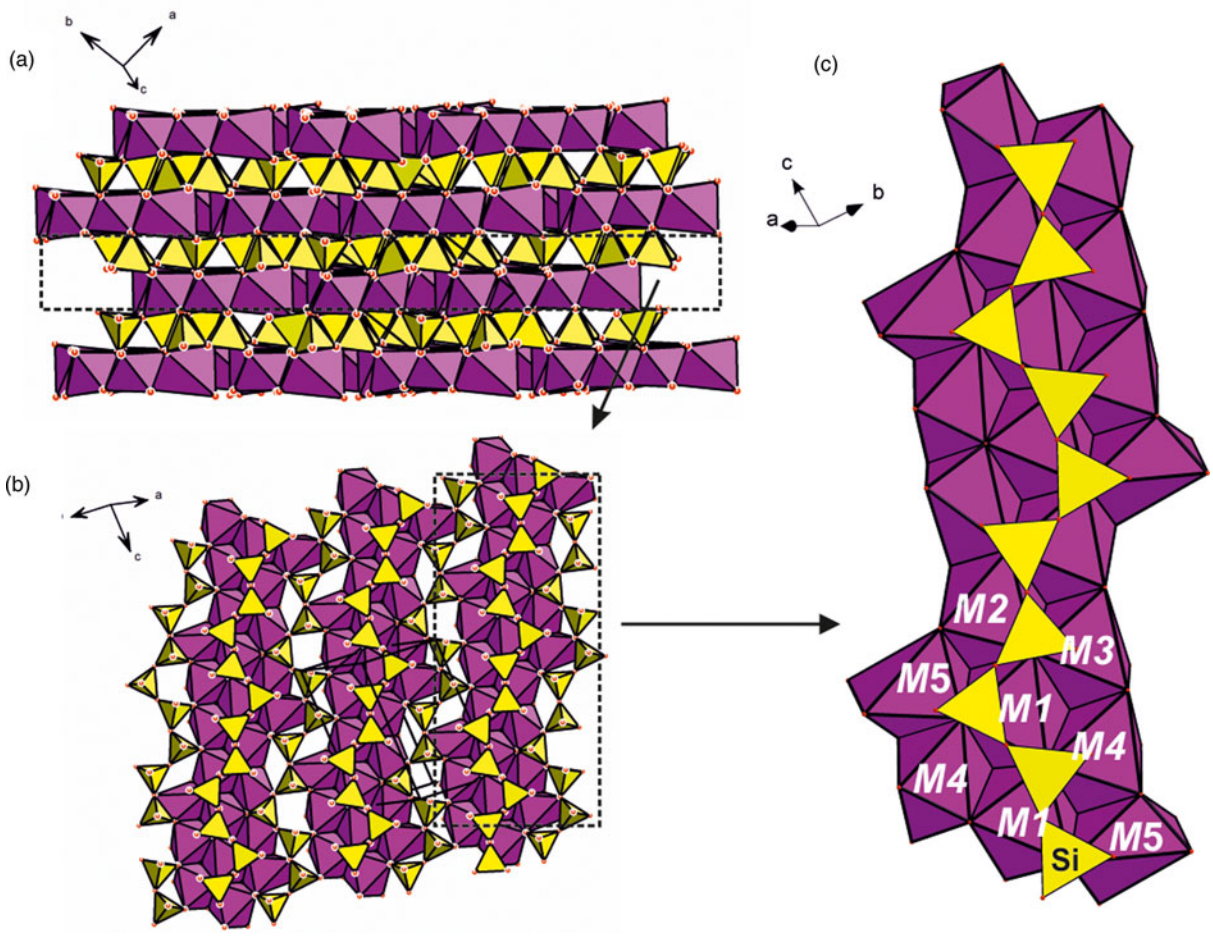

Fig. 3. Crystal structure of vittinkiite (*a* and *b*) and the fragment of polyhedral ribbon with marked sites (*c*). The Mn-centred (*M*) polyhedra are purple and Si-centred tetrahedra are yellow. Dashed lines contour the polyhedral slab (*a*) and polyhedral ribbon (*b*).

https://doi.org/10.1180/mgm.2020.75 Published online by Cambridge University Press

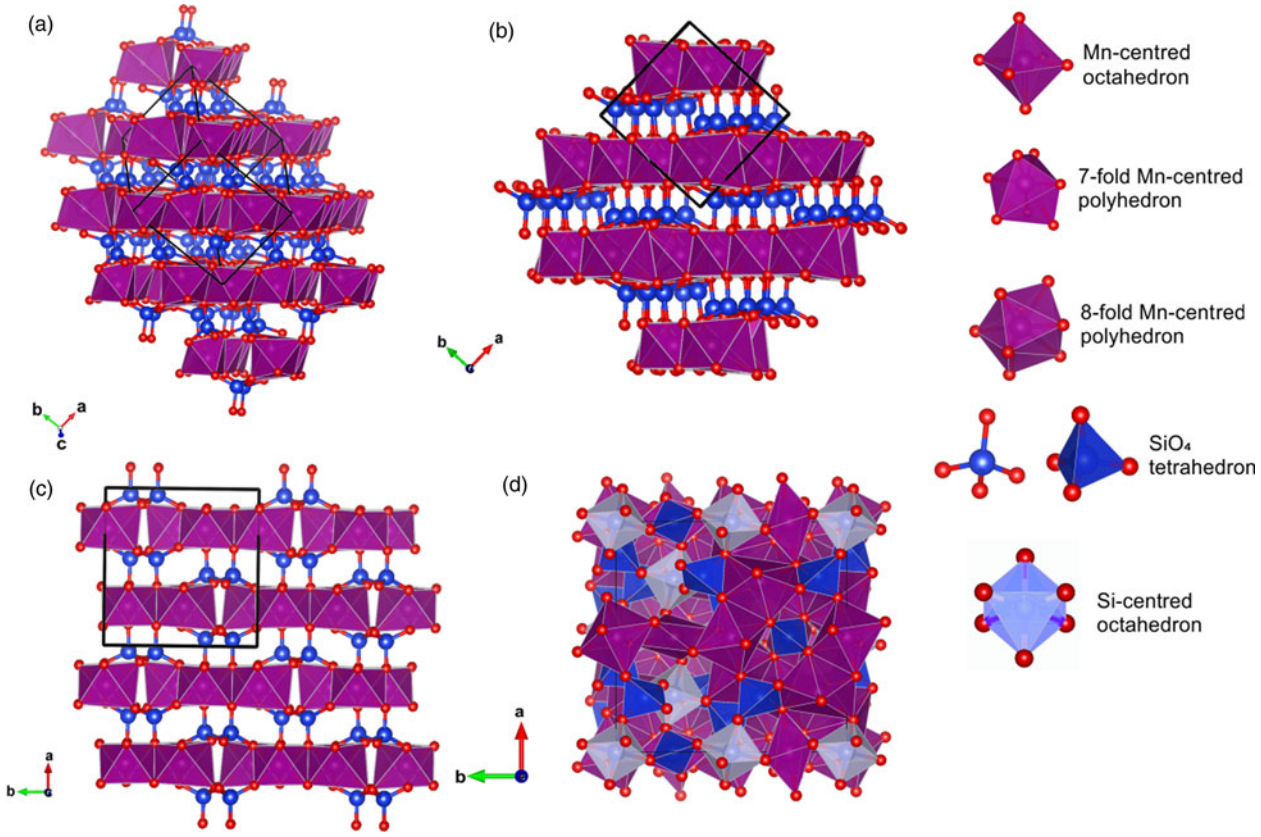

Fig. 4. Projections of crystal structures of $MnSiO_3$ polymorphs: rhodonite type (vittinkiite, this work) (*a*), pyroxmangite (Narita *et al.*, 1977) (*b*), clinopyroxene (Tokohami *et al.*, 1979) (*c*) and tetragonal garnet (Fujino *et al.*, 1986) (*d*). The unit cells are outlined.

The influence of these impurities can be an objective cause of paragenesis of pyroxmangite- and rhodonite-group minerals despite the different fields of stability.

The $MgSiO_3$–$MnSiO_3$ system includes two pyroxenes known in nature: clinopyroxene kanoite, $MnMg[Si_2O_6]$ (Kobayashi, 1977) and orthopyroxene donpeacorite, $(Mn,Mg)MgSi_2O_6$ (Petersen *et al.*, 1984). Gnos *et al.* (1996) showed that rhodonite-group minerals, pyroxmangite, kanoite and donpeacorite can occur together, occasionally forming complex intergrowth. The coexistence of different pyroxenes and pyroxenoids with species-defining Mn, Ca and Mg may indirectly confirm the affinity of their structural types to the species-defining cations and impurities, in which the content and ratios determine the pyroxene or pyroxenoid structural type.

Identification of pyroxenoids with the idealised formula $MnSiO_3$

The occurrence of rhodonite-group minerals (rhodonite, vittinkiite or ferrorhodonite) and pyroxmangite, a pyroxenoid with the generalised formula $(Mn,Fe,Mg,Ca)_7[Si_7O_{21}]$, in paragenesis, despite the difference in their fields of stability, leads to confusion in the identification of these minerals. All of them are important constituents of silicate manganese assemblages, which form at greenschist-facies metamorphism (Roy, 1981; Dasgupta *et al.*, 1990; Brusnitsyn 2000, 2013, 2015; and references therein).

It appears that the end-member polymorphs, vittinkiite and pyroxmangite, were confused during earlier studies in the 'pre-structural' period. Ford and Bradley (1913) noticed that the holotype pyroxmangite was considered initially to be a highly ferrous rhodonite, because most physical properties and chemical features of rhodonite and pyroxmangite are very similar. In the 'pre-structural' period, these minerals were distinguished by optical methods, using 2V and the angle between cleavage planes. The 2V values are different: 63–87° for rhodonite and 37–46° for pyroxmangite (Deer *et al.*, 1978). However, specimens of both rhodonite and pyroxmangite can show a wide variation in 2V ranging from 40 to 72° (Aikawa, 1984, and references therein). Such intermediate values have been explained as due to the submicroscopic lamellar structure of pyroxmangite–rhodonite intergrowths: the thickness of lamellae is smaller than the wavelength used for the measurement of 2V (Aikawa, 1984), which further complicates the identification of these minerals.

The chemical composition of the pyroxenoids discussed cannot be the decisive characteristic for their identification in most common cases because the compositional fields of rhodonite- and pyroxmangite-type pyroxenoids are partially overlapped (Shchipalkina *et al.*, 2019b and references therein). As shown in Fig. 5a, there is a continuous isomorphous series between vittinkiite and rhodonite. The formal border between vittinkiite and rhodonite can be fixed at 0.5 Ca apfu: this is a chemical criterion of subdivision of these mineral species. However, based on literature and our data, we conclude that vittinkiite is not as common in nature as rhodonite (Fig. 5a). Moreover, vittinkiite containing <0.1 Ca apfu is yet unknown. Members of the rhodonite group with 0.4–1.2 Ca apfu are the most widespread in nature. The correlation between contents of Ca and (Mg+Fe) in rhodonite-group minerals is discernible, but indistinctly (Fig. 5a), whereas for

https://doi.org/10.1180/mgm.2020.75 Published online by Cambridge University Press

Table 7. Comparative data for vittinkiite, pyroxmangite and four synthetic polymorphs of $MnSiO_3$.

Structural type	Rhodonite*	Pyroxmangite**	Clinopyroxene	Garnet
Idealised formula	$^{VII(M5)}Mn^{VI(M1-4)}Mn_4[^{IV}Si_5O_{15}]$	$^{VII(M1-2)}Mn^{VI(M3-7)}Mn_5[^{IV}Si_7O_{21}]$	$^{VII(M2)}Mn^{VI(M1)}Mn[^{IV}Si_2O_6]$	$^{VIII}Mn_3\ ^{VI}Mn^{VI}Si[^{IV}SiO_4]_3$
Crystal system	Triclinic	Triclinic	Monoclinic	Tetragonal
Space group	$P\bar{1}$	$P\bar{1}$	$P2_1/c$	$I4_1/a$
Unit-cell parameters				
a (Å); α (°)	6.6980(3); 105.663(3) 6.707(2); 105.40(6)	6.721(2); 113.17(10)	9.864(2)	11.774(1)
b (Å); β (°)	7.6203(3); 92.400(3) 7.616(3); 92.33(6)	7.603(3); 82.27(10)	9.179(2); 108.22(2)	
c (Å); γ (°)	11.8473(5); 94.309(3) 11.851(5); 94.21(6)	17.455(6); 94.13(10)	5.298(1)	11.636(2)
V (Å^3)	579.38(4) 580.90(4)	812.37	455.64	1613.06
Strongest reflections of the powder X-ray diffraction pattern: d(Å)–I(%)	2.75–100 2.94–80 2.96–54 3.14–38 2.18–31 2.60–27 2.66–26 2.98–25 2.08–21 4.74–20	2.67–100 2.99–89 2.98–52 3.13–42 2.18–35 2.60–34 3.01–33 2.65–32 2.23–30 4.77–27	2.95–100 3.07–70 3.28–70 4.68–50 2.18–50 2.63–40 2.50–40 2.19–40 6.56–30 2.52–30	2.63–100 2.62–100 2.94–60 2.60–50 2.90–30 2.39–30 1.57–30 1.56–30 2.14–20 1.63–20
Main bands of the IR spectrum (wavenumbers of maxima, cm^{-1})	1053, 1020, 950, 891, 718, 693, 664, 578, 559	1081, 1045, 1022, 953, 886, 723, 674, 655, 631, 574, 555	no data	no data
References	Narita *et al.* (1977); this work	Narita *et al.* (1977); this work	Akimoto and Syono (1972); Tokonami *et al.* (1979)	Akimoto and Syono (1972); Fujino *et al.* (1986)

*Including the data on vittinkiite and its synthetic analogue
**Including the data on pyroxmangite and its synthetic analogue
Roman numerals in the idealised formula mean the coordination numbers

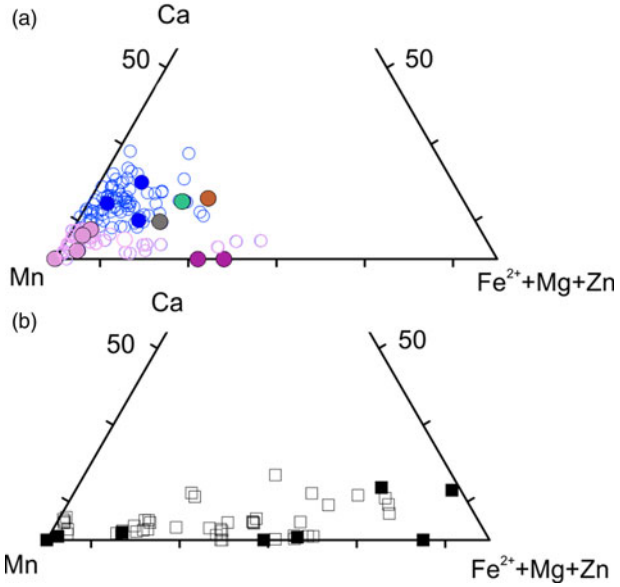

Fig. 5. Ratios of the major metal cations in minerals of the rhodonite group (*a*) and pyroxmangite–pyroxferroite series (*b*), based on literature (Sundius, 1931; Hietanen, 1938; Peacor and Niizeki, 1963; Momoi, 1964; Burnham, 1971; Ohashi and Finger, 1975; Peacor *et al.*, 1978; Sapountzis and Christofides, 1982; Pinckney and Burnham, 1988; Nelson and Griffen, 2005; Shchipalkina *et al.*, 2017; Brusnitsyn, 2000, 2013; 2015; Shchipalkina *et al.*, 2016; and reference therein) and our data. In (*a*) samples with determined crystal structures are marked by filled circles: blue – rhodonite; light purple – vittinkiite; deep purple – synthetic analogue of the end-member vittinkiite; red – ferrorhodonite; green – Zn-rich variety of rhodonite ('fowlerite'); and grey – Mg-enriched variety of rhodonite. Other vittinkiite samples are shown by empty purple circles whereas rhodonite and ferrorhodonite samples are empty blue circles. In (*b*) samples with a determined crystal structure are marked by black (filled) squares.

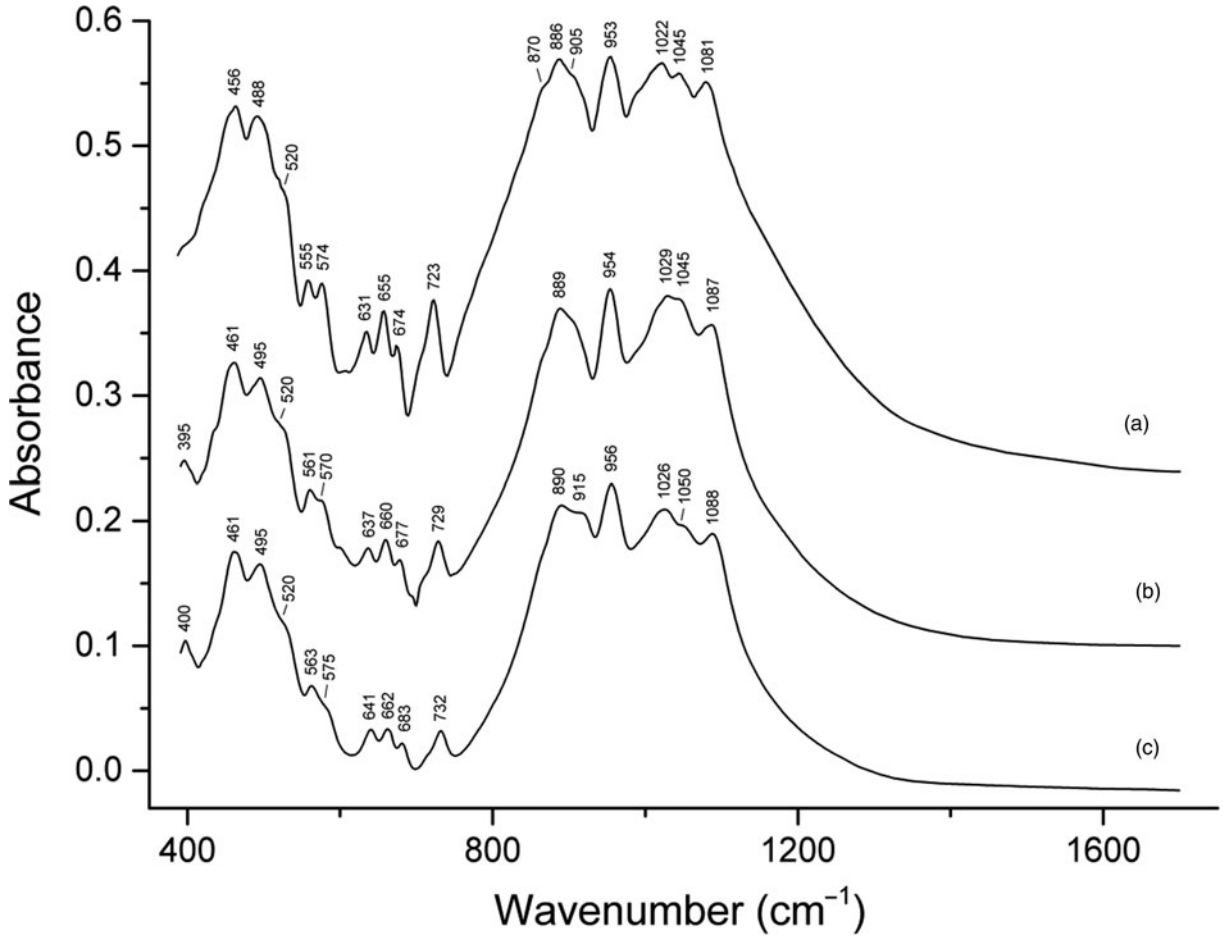

Fig. 6. Infrared absorption spectra of (*a*) Fe-free pyroxmangite with the empirical formula $(Mn_{6.74}Mg_{0.16}Ca_{0.09})(Si_7O_{21})$ from the Southern Faizulinskoe Mn deposit, South Urals, Russia; (*b*) Fe-bearing pyroxmangite with the empirical formula $(Mn_{4.2}Fe_{2.2}Mg_{0.4}Ca_{0.2})(Si_7O_{21})$ from the Razoare Mn deposit, Maramures, Romania; and (*c*) Mn-rich pyroxferroite with the empirical formula $(Fe_{3.0}Mn_{2.8}Mg_{1.1}Ca_{0.1})(Si_7O_{21})$ from a metamorphosed xenolith of gneiss hosted by alkaline basalt of the Bellerberg palaeovolcano, Eifel, Germany.

https://doi.org/10.1180/mgm.2020.75 Published online by Cambridge University Press

pyroxmangite and pyroxferroite this correlation is considerable (Fig. 5b). Generally, there are some regularities in the distribution of Ca, Mg and Fe inherent to rhodonite-group minerals and pyroxmangite occurring together. The content of (Mg+Fe) is higher in pyroxmangite whereas coexisting rhodonite is typically more Ca-rich than pyroxmangite. In general, rhodonite occurs mainly in Mn-bearing rocks enriched in Ca whereas pyroxmangite is more common for Ca-depleted manganolites (Aikawa, 1979; Brusnitsyn, 2000, 2013; 2015 and references therein). However, pyroxmangite and members of the rhodonite–vittinkiite series can occur in intimate intergrowths, typically with lamellar textures (Maresch and Mottana, 1976; Aikawa, 1979, 1984; Brusnitsyn, 2000, 2013, 2015, and references therein).

The most efficient and accurate methods for discrimination of these manganese pyroxenoids are PXRD and IR spectroscopy. The main reflections in the PXRD patterns of rhodonite-group minerals and pyroxmangite appear in the range $d = 3.60–2.50$ Å. However, identification of individual phases in a mixture can be hindered during routine PXRD because of the presence and overlapping of numerous strong reflections in the same region (Brusnitsyn, 2013).

As our data show, vittinkiite (and rhodonite-group minerals in general) and pyroxmangite are distinguished clearly by the IR spectra in the region of 600–700 cm^{-1}. The triplet (631–641) + (655–662) + (674–684) cm^{-1} with the strongest band in the range of 655–662 cm^{-1} is a characteristic feature of pyroxmangite (Fig. 6). In addition, pyroxmangite differs from rhodonite-type minerals in relative intensities of the bands of Si–O stretching vibrations. These features of the IR spectra of pyroxmangite remain for a wide range of the Mn:Fe ratio, up to the point where Fe prevails over Mn, which corresponds to pyroxferroite (Fig. 6). Our study of rhodonite and pyroxmangite specimens from the collection of the Fersman Mineralogical Museum has showed that IR spectroscopy is useful for the identification of individual phases but is not suitable for their mixtures.

Acknowledgements. We thank three anonymous referees for their valuable comments. This work was supported by the Russian Foundation for Basic Research, grant 18-05-00332 (in part for the crystal structure and crystal chemistry of vittinkiite). The infrared spectroscopy investigation was performed in accordance with the state task, state registration No. AAAA-A19-119092390076-7. The technical support by the SPbSU X-Ray Diffraction Resource Center in the powder XRD study is acknowledged.

Supplementary material. To view supplementary material for this article, please visit https://doi.org/10.1180/mgm.2020.75

References

Agilent Technologies (2014) *CrysAlisPro Software system, version 1.171.37.35*. Agilent Technologies UK Ltd, Oxford, UK.

Aikawa N. (1979) Oriented intergrowth of rhodonite and pyroxmangite and their transformation mechanism. *Mineralogical Journal*, **9**, 255–269.

Aikawa N. (1984) Lamellar structure of rhodonite and pyroxmangite intergrowths. *American Mineralogist*, **69**, 270–276.

Akimoto S. and Syono Y. (1972) High pressure transformations in $MnSiO_3$. *American Mineralogist*, **57**, 76–84.

Britvin S.N., Dolivo-Dobrovolsky D.V. and Krzhizhanovskaya M.G. (2017) Software for processing the X-ray powder diffraction data obtained from the curved image plate detector of Rigaku RAXIS Rapid II diffractometer. *Zapiski Rossiiskogo Mineralogicheskogo Obshchestva*, **146**, 104–107 [in Russian].

Brusnitsyn A.I. (2000) *Rhodonite Deposits of Middle Urals (Mineralogy and Genesis)*. St. Petersburg University, Russia [in Russian].

Brusnitsyn A.I. (2013) *Mineralogy of Manganese Metasedimentary Rocks of South Urals*. St. Petersburg University, Russia, 153 pp. [in Russian].

Brusnitsyn A.I. (2015) *Parnokskoe Manganese Deposit, Polar Urals: Mineralogy, Geochemistry and Genesis of Ores*. St. Petersburg University, Russia, 116 pp. [in Russian].

Brusnitsyn A.I. and Zaitsev A.N. (2000) Rhodonite as a new mineral. *Urals Summer Mineralogical School – 2000*. UGGGA, Ekaterinburg, Russia, pp. 38–41 [in Russian].

Burnham C.W. (1971) The crystal structure of pyroxferroite from Mare Tranquillitatis Locality: Apollo 11 microgabbro sample 10047, Mare Tranquillitatis, Moon. *Proceedings of the Second Lunar Science Conf. on Proceedings of the Second Lunar Science Conference*, **1**, 47–57.

Chukanov N.V. (2014) *Infrared Spectra of Mineral Species: Extended Library*. Springer Verlag. Dordrecht, The Netherlands, 1726 pp.

Dasgupta S., Banerjee H., Fukuoka M. and Bhattacharya Roy S. (1990) Petrogenesis of Metamorphosed manganese deposits and the nature of the precursor sediments. *Ore Geology Reviews*, **5**, 359–384.

Deer W.A., Howie R.A. and Zussman J. (1978) *Rock-Forming Minerals. V. 24*, John Wiley and Sons Inc., New York.

Ford W.E. and Bradley W.M. (1913) Pyroxmangite, a new member of the pyroxene Group and its alteration product, skemmatite. *American Journal of Science*, **186**, 169–174.

Fujino K., Momoi H., Sawamoto H. and Kumazawa M. (1986) Crystal structure and chemistry of $MnSiO_3$ tetragonal garnet. *American Mineralogist*, **71**, 781–785.

Germar H. (1819) Ueber die kohlenstoff – und kieselsauren Manganerze des Unterharzes. *Journal für Chemie und Physik*, **26**, 108–120.

Gnos E., Armbruster T. and Nyfeler D. (1996) Kanoite, donpeacorite and tirodite: Mn-Mg-silicates from a manganiferous quartzite in the United Arab Emirates. *European Journal of Mineralogy*, **8**, 251–261.

Henry M. (1998) Retrosynthesis in inorganic crystal structures: application to nesosilicate and inosilicate networks. *Coordination Chemistry Reviews*, **178–180**, 1109–1163.

Hietanen A (1938) On the petrology of Finnish quartzites. *Bulletin de la Commission Géologique de Finlande*, **122**, 1–119.

Ibers J.A. and Hamilton W.C. (editors) (1974) *International Tables for X-Ray Crystallography*. Vol. **IV**. The Kynoch Press, Birmingham, UK, 366 pp.

Ito J. (1972) Rhodonite–pyroxmangite peritectic along the join $MnSiO_3$-$MgSiO_3$ in air. *American Mineralogist*, **57**, 865–876.

Jasche C.F. (1817) Das Rothmanganerz in der Gegend von Elbingerode am Harz. *Kleine Mineralogische Schriften*, **1**, 1–19.

Kobayashi H. (1977) Kanoite, $(Mn^{2+},Mg)_2[Si_2O_6]$, a new clinopyroxene in the metamorphic rock from Tatchira, Oshima Peninsula, Hokkaido, Japan. *Journal of Geological Society of Japan*, **8**, 537–542.

Koto K., Morimoto N. and Narita H. (1976) Crystallographic relationships of the pyroxenes and pyroxenoids. *Journal of Japanese Association of Mineralogy, Petrology and Economic Geology*, **71**, 248–254.

Leverett P., Williams P.A. and Hibbs D.E. (2008) Ca-Mg-Fe-rich rhodonite from the Morro da Mina mine, Conselheiro Lafaiete, Minas Gerais, Brasil. *The Mineralogical Record*, **44**, 149–184.

Liebau F. (1962) Die Systematik der Silikate. *Naturwissenschaften*, **49**, 481–491.

Liebau F., Hilmer W. and Lindemann G. (1959) Über die Kristallstruktur des Rhodonit (Mn,Ca)SiO_3. *Acta Crystallographica*, **12**, 182–187.

Maresch W.V. and Mottana A. (1976) The pyroxmangite-rhodonite transformation for the $MnSiO_3$ composition. *Contribution to Mineralogy and Petrology*, **55**, 69–79.

Momoi H. (1964) Mineralogical study of rhodonites in Japan, with special reference to contact metamorphism. *Memoirs of the Faculty of Science Kyushu University, Series D.*, **15**, 39–63.

Momoi H. (1974) Hydrothermal crystallization of $MnSiO_3$ polymorphs. *Mineralogical Journal*, **7**, 359–373.

Miyawaki R., Hatert F., Pasero M. and Mills S.J. (2019) Newsletter 49. New minerals and nomenclature modifications approved in 2019. IMA Commission on New Minerals, Nomenclature and Classification (CNMNC). *Mineralogical Magazine*, **83**, 479–483, p. 483.

Morimoto N., Koto K. and Shinohara T. (1966) Oriented transformation of johannsenite to bustamite. *Mineralogical Journal*, **5**, 44–64.

Narita H. (1973) *Crystal Chemistry of Pyroxene and Pyroxenoid Polymorphs of $MnSiO_3$*. Doctoral Thesis, Osaka University, Osaka, Japan.

Narita H., Koto K. and Morimoto N. (1977) The crystal structures of $MnSiO_3$ polymorphs (rhodonite- and pyroxmangite-type). *Mineralogical Journal of Sapporo*, **8**, 329–342.

Nelson W.R. and Griffen D.T. (2005) Crystal chemistry of Zn-rich rhodonite ("fowlerite"). *American Mineralogist*, **90**, 969–983.

Nordenskiöld A.E. (1863) *Beskrifning öfver de i Finland funna mineralier*. P. Th. Stolpes förlag, Helsingfors [Helsinki], (2nd edition), 177 pp. [in Swedish].

Ohashi Y. and Finger L.W. (1975) Pyroxenoids: a comparison of refined structures of rhodonite and pyroxmangite. *Carnegie Institution of Washington Year Book*, **74**, 564–569.

Peacor D.R. and Niizeki N. (1963) The redetermination and refinement of the crystal structure of rhodonite. $(Mn.Ca)SiO_3$. *Zeitschrift für Kristallographie*, **119**, 98–116.

Peacor D.R., Essene E.J., Brown P.E. and Winter G.A. (1978) The crystal chemistry and petrogenesis of a magnesian rhodonite. *American Mineralogist*, **63**, 1137–1142.

Pertlik F. and Zahiri R. (1999) Rhodonite with a low calcium content: crystal structure determination and crystal chemical calculations. *Monatshefte fur Chemie*, **130**, 257–265.

Petersen E.U., Anovitz L.M. and Essene E.J. (1984) Donpeacorite, $(Mn,Mg)MgSi_2O_6$, a new orthopyroxene and its proposed phase relations in the system $MnSiO_3$–$MgSiO_3$–$FeSiO_3$. *American Mineralogist*, **69**, 472–480.

Petříček V., Dušek M. and Palatinus L. (2006) *Jana2006. Structure Determination Software Programs*. Institute of Physics, Praha, Czech Republic.

Pinckney L.R. and Burnham C.W. (1988) Effects of compositional variation on the crystal structures of pyroxmangite and rhodonite. *American Mineralogist*, **73**, 798–808.

Ross C.S. and Kerr P.F. (1932) The manganese minerals of a vein near Bald Knob, North Carolina. *American Mineralogist*, **17**, 1–18.

Roy S. (1981) *Manganese Deposits*. Academic Press, London.

Sapountzis E.S. and Christofides G. (1982) A calcium-poor rhodonite from Xanthi (N. Greece). *Mineralogical Magazine*, **46**, 337–340.

Shchipalkina N.V., Aksenov S.M., Chukanov N.V., Pekov I.V., Rastsvetaeva R.K., Schafer C., Ternes B. and Schuller W. (2016) Pyroxenoids of pyroxmangite-pyroxferroite series from xenoliths of Bellerberg paleovolcano (Eifel, Germany): chemical variations and specific features of cation distribution. *Crystallography Reports*, **61**, 931–939.

Shchipalkina N.V., Chukanov N.V., Pekov I.V., Aksenov S.M., McCammon C., Belakovskiy D.I., Britvin S.N., Koshlykova N.N., Schafer C., Scholz R. and Rastsvetaeva R.K. (2017) Ferrorhodonite $CaMn_3Fe[Si_5O_{15}]$, a new mineral species from Broken Hill, New South Wales, Australia. *Physics and Chemistry of Minerals*, **44**, 323–334.

Shchipalkina N.V., Pekov I.V., Chukanov N.V., Zubkova N.V., Belakovskiy D.I., Britvin S.N. and Koshlyakova N.N. (2019a) Vittinkiite, IMA 2017-082a. CNMNC Newsletter No. 51; *Mineralogical Magazine*, **83**, 757–761.

Shchipalkina N.V., Pekov I.V., Chukanov N.V., Biagioni C. and Pasero M. (2019b) Nomenclature of minerals of the rhodonite group. *Mineralogical Magazine*, **83**, 829–835.

Sundius N. (1931) On the triclinic manganiferous pyroxenes. *American Mineralogist*, **16**, 411–429, 488–518.

Takeuchi Y. (1977) Designation of cation sites in pyroxenoids. *Mineralogical Journal*, **8**, 431–438.

Tokohami M., Horiuchi H., Nakano A., Akimoto S.I. and Morimoto N. (1979) The crystal structure of the pyroxene-type $MnSiO_3$. *Mineralogical Journal (Japan)*, **9**, 424–426.

https://doi.org/10.1180/mgm.2020.75 Published online by Cambridge University Press